Heliyon 6 (2020) e04505

Contents lists available at ScienceDirect

Heliyon

journal homepage: www.cell.com/heliyon

Research article

Morphological variations in Bi_2S_3 nanoparticles synthesized by using a single source precursor

Damian C. Onwudiwe [a,b,*], Violet M. Nkwe [a,b]

[a] Material Science Innovation and Modelling (MaSIM) Research Focus Area, Faculty of Agriculture, Science and Technology, North-West University (Mafikeng Campus), Private Bag X2046, Mmabatho, South Africa

[b] Department of Chemistry, School of Physical and Chemical Sciences, Faculty of Natural and Agricultural Science, North-West University (Mafikeng Campus), Private Bag X2046, Mmabatho, South Africa

ARTICLE INFO

Keywords:
Materials chemistry
Inorganic chemistry
Bismuth sulphide
Solvothermal
Morphology
Structural properties
Bismuthinite

ABSTRACT

A simple solvothermal decomposition of bismuth dithiocarbamate complex in oleylamine, oleic acid, and hexadecylamine at 180 °C, yielded bismuth sulphide nanomaterials of different morphologies represented as Bi_2S_3(OAm), Bi_2S_3(OAc) and Bi_2S_3(HDA) respectively. The bismuth complex, used as the single source precursor, was synthesized and characterised by elemental analysis, FTIR, and NMR spectroscopic techniques. The spectroscopic and micro analysis confirmed the proposed compound, while the as-prepared nanoparticles were characterized using UV-visible spectroscopy, X-ray diffraction (XRD), scanning electron microscopy (SEM), transmission electron microscopy (TEM), and energy dispersive spectrometer (EDS). The effects of the different solvent media on the structural properties of the obtained Bi_2S_3 were investigated. An orthorhombic phase bismuthinite of varying intensities were obtained, with an indication that a bias of orientations existed in the (2 1 1) crystallographic planes in the Bi_2S_3(OAm) compared to the characteristic (1 3 0) diffraction peak of Bi_2S_3. The microscopic analysis showed a correlation between the nanoparticles' morphology and the type of solvent used, which also implied that the properties of Bi_2S_3 were affected by the solvent medium.

1. Introduction

Metal sulphides are particularly attractive within the broad family of functional materials due to their wide applications in electronic, energy storage and conversion, optics and biomedical fields [1, 2, 3, 4]. They have unique optical and structural properties, and have also found application in electrochemical detection and photocatalysis [5, 6, 7].

The synthesis of nanocystalline materials and the manipulation of their synthesis conditions in order to obtain materials with different properties is one of the interesting research aspects that is being explored recently [8, 9, 10]. This is because morphology, dimensionality, crystallinity, and chemical composition of nanostructured materials profoundly influence their physicochemical properties and applications. Thus, the optical and structural properties of nanomaterials ultimately depend on the methods and conditions of preparation [11,12]. Achieving a narrow size distribution in addition to a well-defined morphology are the two parameters that allow the modification of fundamental properties of nanoparticles; thereby enhancing the efficiency of their performance for applications in various areas [13,14].

Different methods of wet chemical processes have been used to afford series of isotropic and anisotropic chalcopyrite nanocrystalline materials such as spherical, star-like, flower-like, nanorods/wires/tube, and nanofibers [12, 15, 16, 17, 18, 19]. Solvothermal method has emerged as one of the wet chemical routes that offer better control on the preparation of different nanostructures in different media [16]. Solvents play important role during reaction process and in nanoparticles preparation; the role may include temperature control, surface passivation, regulating the particle growth and coarsening, controlling NPs shape, size, aspect ratio and size distribution [20]. The solvent, thus, provides means of achieving control over the nanoparticles, which influences the different properties of nanomaterials for specific applications [21].

Among the different solvents used in the synthesis of nanoparticles, oleylamine, oleic acid and hexadecylamine are well-known for their extensive use as capping agents in synthesis. This is due to their high boiling point, good coordinating property, and high chemical and thermal stability even up to their boiling points (330–360 °C). Due to the good coordinating potential of their ligating atoms (O and N), they have high tendency to form complexes with the metal at intermediate

* Corresponding author.
E-mail address: Damian.Onwudiwe@nwu.ac.za (D.C. Onwudiwe).

https://doi.org/10.1016/j.heliyon.2020.e04505
Received 17 March 2020; Received in revised form 13 May 2020; Accepted 15 July 2020

temperatures, which allows a controlled decomposition of the metal-OAm/OAc/HDA complex to produce nanoparticles.

Bismuth sulphide is a p-type semiconductor with multiple intrinsic properties, such as low direct energy band gap of 1.3 eV, high ionic conductivity, high absorption coefficient (10^4–10^5 cm^{-1}) and a good incident photon to electron conversion efficiency (~5%) [22,23]. It is a unique material whose structure is made up of a lamellar arrangement of Bi^{3+} and S^{2-} in alternating infinite chains [23]; and it prefers the orthorhombic system when it crystallizes out [23, 24, 25]. These properties, in addition to its non-toxicity makes it an attractive material in different fields of applications such as energy storage [26], photovoltaics [27] and in the removal of pigments from water [28]. Research on Bi_2S_3 has increased recently due to its structural flexibility, since the morphology of a semiconductor remains an important factor when considering their application.

Bismuth sulphide nanostructures of different morphologies have been fabricated by various approaches using different solvents as capping agents and also to direct the growth of the nanomaterials towards different anisiotropic patterns. Sarkar et al. [29] reported diverse morphologies of Bi_2S_3 including nanospheres, nanorods and hexagonal nanostructures, prepared by solvothermal decomposition of Bi(III) dithiocarboxylate complex in various solvents. Thioglycolic acid (TGA) has been used as a capping agent to prepare hierarchical nanostructures of Bi_2S_3, with thioacetamide as the sulphur source [30]. Using TGA as both the sulphur source and stabilising agent in a hydrothermal process, Salavati-Niasari et al. [31] synthesized Bi_2S_3 nanostructures with different morphologies including nanoflower, nanorod and nanobelt. Polyol was used as passivating agent to prepare some flake-like and rod-like Bi_2S_3 nanostructures in a simple refluxing process [32]. Due to the ability of gelatine to complex to metal ions via their polar groups and influence the assembly and morphology of inorganic nanostructures, it has been used to prepare Bi_2S_3 nanorods under microwave irradiation [27]. The single source precursor route offers the benefits of a single step reaction with relatively easy to manipulate synthesis conditions. Compared to the multiple source precursors approach, it has the advantage of containing both elements that are required in the desired product. Therefore, a better control of stoichiometry is guaranteed and there is no need for pre reactions or the use of toxic gases such as H_2S [33]. The use dithiocarbamate as single-source precursors for the synthesis of nanoscale metal sulphides is well established [34]. This has been ascribed to their easy synthesis process and clean thermal decomposition [35, 36, 37, 38, 39, 40]. In this research, bismuth(III) tris (*N*-methyl--*N*-phenyl dithiocarbamate) has been used as a single source precursor to prepare different nanostructures of Bi_2S_3 by solvothermal method in oleylamine, oleic acid and hexadecylamine as capping molecules.

2. Experimental section

2.1. Chemicals

Bismuth(III) nitrate pentahydrate ($Bi(NO_3)_3 \cdot 5H_2O$), N-methylaniline, hexadecylamine (HDA), oleic acid (OAc) and 1-oleylamine (OAm) were obtained from Merck chemicals. Analytical grade toluene, methanol, and ethanol were purchased from Alfa Chemical Co.

2.2. Synthesis of bismuth(III) tris(N-methyl-N-phenyldithiocarbamate)

$Bi(NO_3)_3 \cdot 5H_2O$ (1.30 g, 0.003 mol) was suspended in 50 mL water. To this, was added few drops of concentrated HCl until a clear solution was obtained and then followed by 12 mL aqueous solution of ammonium *N*-methyl-*N*-phenyldithiocarbamate (0.001 mol). The mixture was stirred for 1 h and the yellow solid obtained was filtered and rinsed thoroughly with ethanol/water. Pure product was obtained by dissolving in chloroform, filtering and then recrystallizing the product.

Yield: 64%, M.p. 203–206 °C. ^{1}H NMR ($CDCl_3$) δ = 7.41–7.28 (m, 10H, $–C_6H_5$), 3.67 (s, 6H, $N–CH_3$). ^{13}C NMR ($CDCl_3$) δ 145.82, 129.55, 128.23, 126.50($-C_6H_5$), 45.69($-CH_3$), 205.05($-CS_2$). Selected IR, υ(cm^{-1}): 1489 (C=N), 1362 (C_2–N), 1002 (C=S), 3010 (=CH), 2923(–CH). Anal. Calc. for $C_{24}H_{24}N_3S_6Bi$(755.84): C, 38.14; H, 3.20; N, 5.56; S, 25.45. Found: C, 38.60; H, 3.40; N, 5.10; S, 24.70.

2.3. Synthesis of Bi_2S_3 nanostructures

All experiments were carried out by heat-up method under N_2 atmosphere [41]. In a typical synthesis, 0.25 g of bismuth(III) tris(*N*-methyl-*N*-phenyldithiocarbamate) was added into a 10 mL oleylamine (OAm) in a round bottom flask with a condenser. After stirring at room temperature for 15 min, the mixture was then degassed for 10 min and then backfilled with nitrogen. This process was repeated twice, and then the mixture was heated steadily to 180 °C and maintained for 1 h. Afterwards, the dark solution was cooled down to room temperature, and the product was separated by the addition of methanol and centrifugation. Purification of the product was carried out by centrifugation using a mixture of toluene and ethanol (1:3 v/v) and repeating the process four times to ensure complete removal of the excess capping agent. The same process was repeated using oleic acid (OAc) and hexadecylamine (HDA) as solvent, and in each case the final products were dispersed in 15–20 mL toluene to obtain stable solutions.

2.4. Characterization

The complex, bismuth(III) tris(*N*-methyl-*N*-phenyldithiocarbamate), was characterized using Alpha Bruker FTIR spectrophotometer for the identification of functional groups. Elementar, Vario EL Cube for the analysis of the percentage C, H, N, and S, and a Bruker Avance III NMR spectrophotometer (600 MHz) for the (^{1}H and ^{13}C) NMR measurement in chloroform. The as-synthesized nanostructures were characterized by X-ray diffraction using a Bruker AXS D_8 Discover XRD (Cu KÎ = 1.5406A) X-ray diffractometer operated at 40 KV and 40 mA. The UV-vis-NIR absorption spectra of the nanostructures solutions were measured in toluene using a Perkin Elmer Lambda 750S UV-vis-NIR spectrophotometer. A JEOL JEM 2100 High Resolution Transmission Electron Microscope (HRTEM) was used for TEM imaging. This was done at an accelerating voltage of 200 kV. Spatula tips of samples were dispersed in ethanol and sonicated for 30 min and allowed to dry for a few minutes prior to analysis. Scanning electron microscope (SEM) analysis was carried out using a FEI Quanta FEG 250 Environmental Scanning electron microscope (ESEM), and the elemental composition was determined using Oxford X-map 20 detector at 15 kV and using INCA software for energy dispersive X-ray analysis (EDAX).

3. Results and discussion

3.1. Spectral studies of the bismuth complex

The FTIR spectrum of the complex show ν(C–N) (thioureide) peak at 1489 cm^{-1}. The position of this band, typical of dithiocarbamates, indicated a partial double bond character [42]. The bond energy falls between the single (1350–1250 cm^{-1}) and double (1690–1650 cm^{-1}) bond energies. Only one signal appeared around 1002 cm^{-1} due to the ν(C–S), supporting a bidentate coordination fashion of the dithiocarbamate ligand [43].

^{1}H and ^{13}C NMR spectra of the complex are shown in Figure 1. The ^{1}H NMR spectrum exhibits a signal around 3.67 ppm for the CH_3 protons attached to the nitrogen atom of the dithiocarbamate. A multiplet in the range 7.28–7.41 ppm is attributed to the phenyl protons. Apart from these signals, the peak at 1.55 ppm is due to the residual water peak. The $^{13}CS_2$ chemical shifts reveal a weak signal, which is usually associated with the backbone carbon ($N^{13}CS_2$), at 205.0 ppm. The $N^{13}CS_2$ carbon

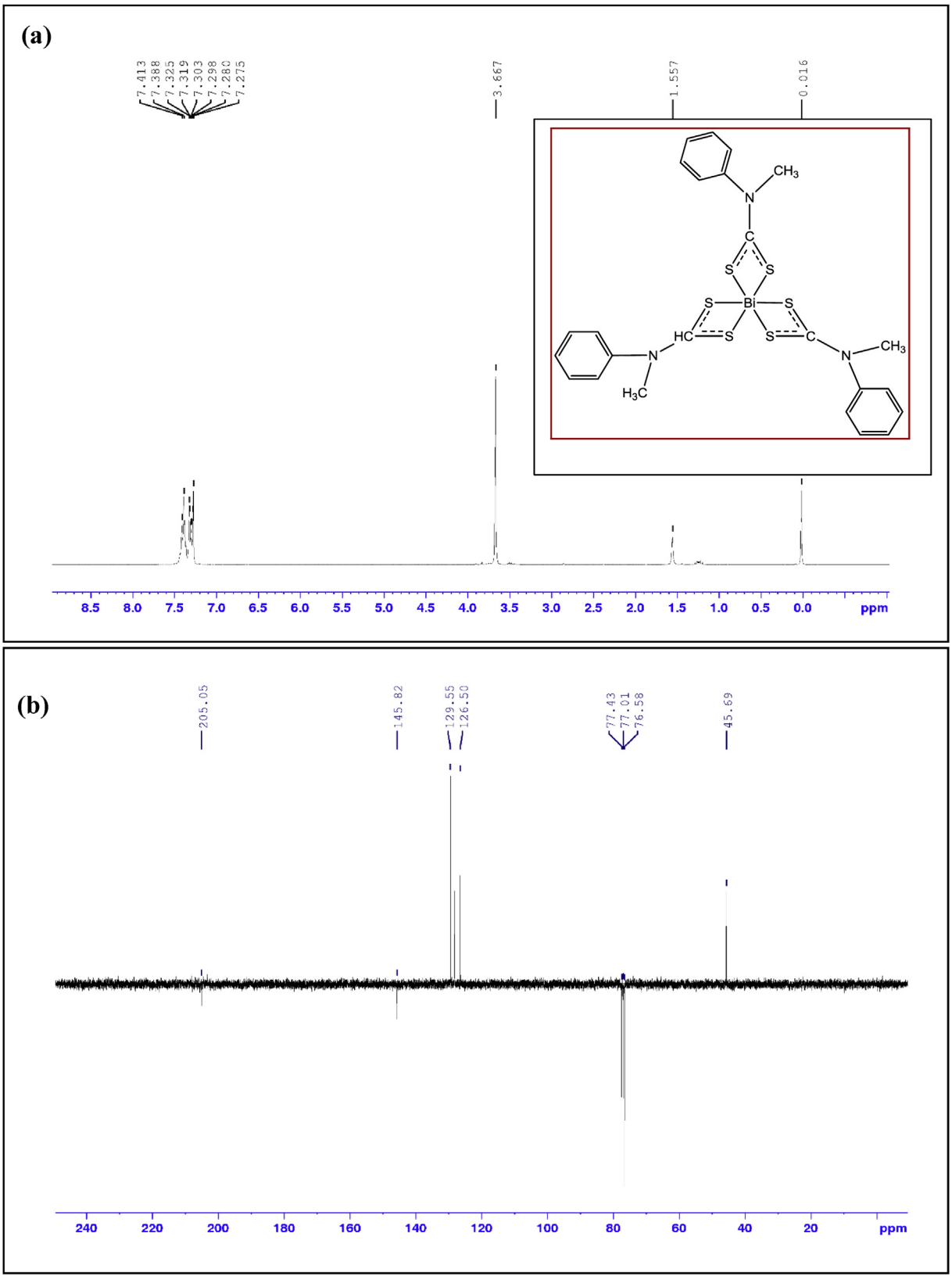

Figure 1. (a) ^{1}H and (b) ^{13}C NMR spectra of the bismuth(III) tris(*N*-methy-*N*-phenyl dithiocarbamate) complex.

signals for phenyl ring were observed at 145.82, 129.55, 128.23, 126.50 ppm. The carbon signals due to the methyl proton associated with the N-substituted groups of the dithiocarbamate resonated at relatively low field around 45.69 ppm; and may be attributed to the electronegativity of the nitrogen atom and the presence of the aromatic ring.

3.2. Synthesis of bismuth sulphide

The nanostructured Bi_2S_3 were synthesized using OAm, OAc and HDA as capping ligand while bismuth(III) tris(*N*-methyl-*N*-phenyl-dithiocarbamate) was the precursor complex. The nucleation of Bi_2S_3

occurred upon the decomposition of the metal complex and subsequent growth or assembly into nanostructures at the reaction temperature. At the optimum reaction temperature of 180 °C, the precursor complex completely decomposed and phase pure Bi_2S_3 nanostructures were formed. Crystal formation has been reported to be controlled by kinetic and thermodynamic growth factors, of which the type of precursor compounds, nature of capping agents and the reaction temperature predominantly govern the morphology and crystalline phase of the product [44,45]. The effect of the solvent types on the crystal structure and morphology of the synthesized Bi_2S_3 samples were investigated using XRD, SEM, and TEM. In the formation mechanism of the different morphologies, the reaction commenced with the development of weak coordination by the capping ligand to the surface of the bismuth complex at elevated temperature. As the reaction progressed, with increase in temperature, the decomposition of the complex was followed with nucleation which resulted in Bi_2S_3 nuclei. The growth pattern/rate of the nuclei and likely aggregation into different nanostructures was dependent on the type of capping agent used and the coordinating potency.

3.3. Structural analysis

The XRD patterns of the Bi_2S_3(OAm), Bi_2S_3(OAc), and Bi_2S_3(HDA) are presented in Figure 2(a)–(c) respectively. All the patterns showed peaks at 2θ values of 24.9°, 28.6°, 31.8°, 39.8°, and 46.5°, which were assigned to the diffraction line produced by (130), (211), (221), (141), and (431) planes; and were attributed to orthorhombic phase bismuthinite Bi_2S_3 (JCPS 00-017-0320), with space group Pbnm. One of the important aspects revealed from these patterns was the difference in the intensity of the diffraction peaks based on the type of capping agents used. In Bi_2S_3(OAm), they seem to be a significant intensification of the (2 1 1)

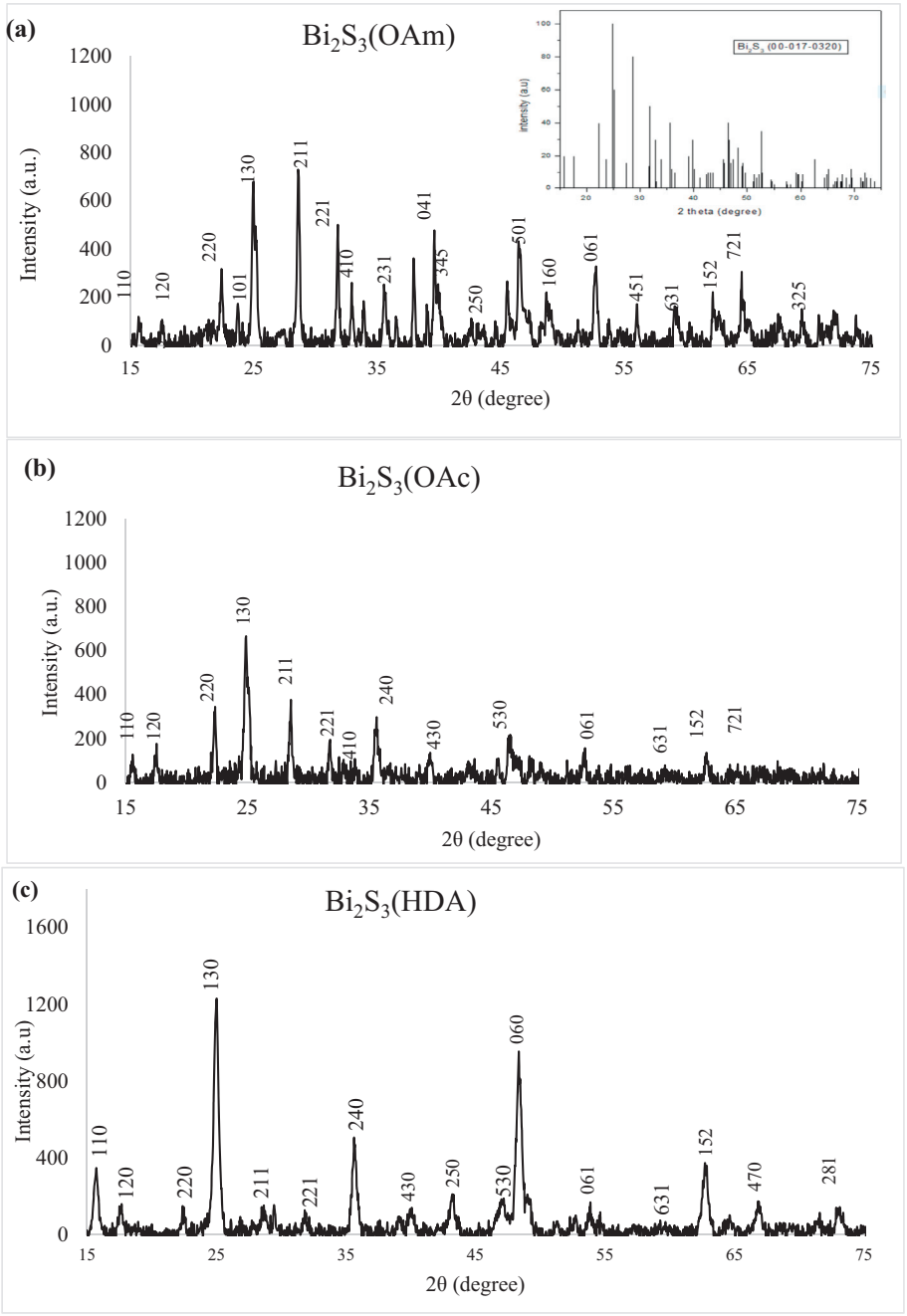

Figure 2. XRD patterns of Bi_2S_3 synthesized by the thermal decomposition of bismuth(III) tris(*N*-methyl-*N*-phenyldithiocarbamate) in (a) oleylamine, (b) oleic acid, and (c) hexadecylamine.

peak, compared with the characteristic (1 3 0) diffraction peak of Bi_2S_3. This was an indication that there existed a bias of orientations of these crystallographic plane [31].

The ratio of the intensities of the (211) to the (130) diffraction peak, I(211)/I(130), of Bi_2S_3(OAm), Bi_2S_3(OAc), and Bi_2S_3(HDA)were obtained as 1.02, 0.57 and 0.09 respectively. The smaller ratio values obtained for Bi_2S_3(OAc) and Bi_2S_3(HDA) compared to the value for standard Bi_2S_3 is suggestive of a (130) preferred orientation, contrary to the orientation of the Bi_2S_3(OAm) with a significantly higher value. This might be attributed to the growth of Bi_2S_3 nanorods, which usually show a preferential direction along the c-axis due to its intrinsic crystal structure [46]. Studies have shown that Bi_2S_3 possesses a lamellar structure in which the Bi_2S_3 units are linked in such a way that they form infinite chains that are parallel to the c-axis and are joined via weaker van der Waals interactions [47,48]. The enhanced growth rate along the c-axis is facilitated by a stronger covalent bond between the planes which are perpendicular to the c-axis.

3.4. Morphological studies

Figures 3, 4, and 5 demonstrate the SEM and TEM micrographs of the synthesized Bi_2S_3 nanoparticles in oleylamine, oleic acid and hexadecylamine respectively. The figure illustrates the effect of the different solvents on the morphology of the synthesized Bi_2S_3. The SEM micrographs of Bi_2S_3(OAm) (Figure 3a) showed short rods embedded in interlocking sheets, while the TEM image showed distinct rods with an average diameter of 46 nm and length of 128 nm, shown in the particle size distribution histogram in the inset of Figure 3b. The SEM and TEM micrographs of Bi_2S_3(OAc) in Figure 4a and b respectively, show predominantly spherical shape of Bi_2S_3. The particle size was calculated from the TEM image by considering a reasonable number of the particles and plotting their size histogram as shown in the inset of Figure 4b. An average size of 28 nm was obtained. A flower-like morphology was obtained for the Bi_2S_3(HDA) sample as shown in the SEM image of Figure 5a, which also appeared as agglomeration of interlocked ultrathin fine structures in the TEM micrograph (Figure 5b). The HRTEM images of the three samples, presented in Figures 3c, 4c and 5c, indicated that the particles were crystalline with Bi_2S_3(OAm) displaying the highest crystallinity.

The suitability and versatility of oleylamine as the reaction medium has been demonstrated for a broad range of nanomaterials in chemical synthesis [49]. OAm has been reported to work not only as a stabilizer for the oriented growth of nanoparticles, but also acts as a catalyst, thereby accelerates the thermal decomposition of precursors. Therefore, it controls both nucleation and growth kinetics processes [49]. It combines its roles as solvent and surfactant, with its suitability as reducing agent in materials synthesis. Unlike hexadecylamine which is solid at room temperature, OAm has advantage of existing in liquid state and is easily removed by centrifugation.

The variation in morphology of nanoparticles during the solvothermal process, could be attributed to their growth mechanisms. This is dependent on the capping agent, which acts by suppressing the growth of certain crystal facet via coordination to the metal cations [50]. The properties of the capping agents have been reported to play important role in controlling both the size and morphology of nanoparticles [51]. The growth of nanostructures is dependent on Ostwald ripening and oriented attachment. Capping agents can largely influence the oriented attachment processes since they directly modify the nanostructures surface [52]. The different capping agents used have different molecular weight, and this also influences the pattern of assembly of the capped nanoparticles. In the presence of the capping ligands, the mechanism by which the nanoparticles growth proceeds largely depend on the nature of the capping ligands, the concentration of the monomer that is formed, in addition to the amount of the capping agent that is present to prompt nucleation. While the growth of the monomer attachment characteristically gives the best route for the formation of single crystalline materials, the coalescence growth typically leads to nanoparticles which have multiple twin structures including high-energy facets [53]. The functional groups of the capping agents are different from one other. For example, oleic acid has a carboxylic acid functional group, HDA and oleylamine possess an ammine end and, in addition, both of them have double bond between C-9 and C-10. The capping agents form coordination bond with Bi^{3+} ion and are able to modify the size and morphology of Bi_2S_3 nanoparticles during crystal growth in the solvothermal system. Due to the high electronegativity of the reacting sites of oleic acid, the molecules could orient and attach to the surface of the nanoparticles with its –OH group during the synthesis process. This is possible since the molecules are capable of approaching the Bi_2S_3 surface at all facets (along all axis and all planes); consequently, resulting in the formation of

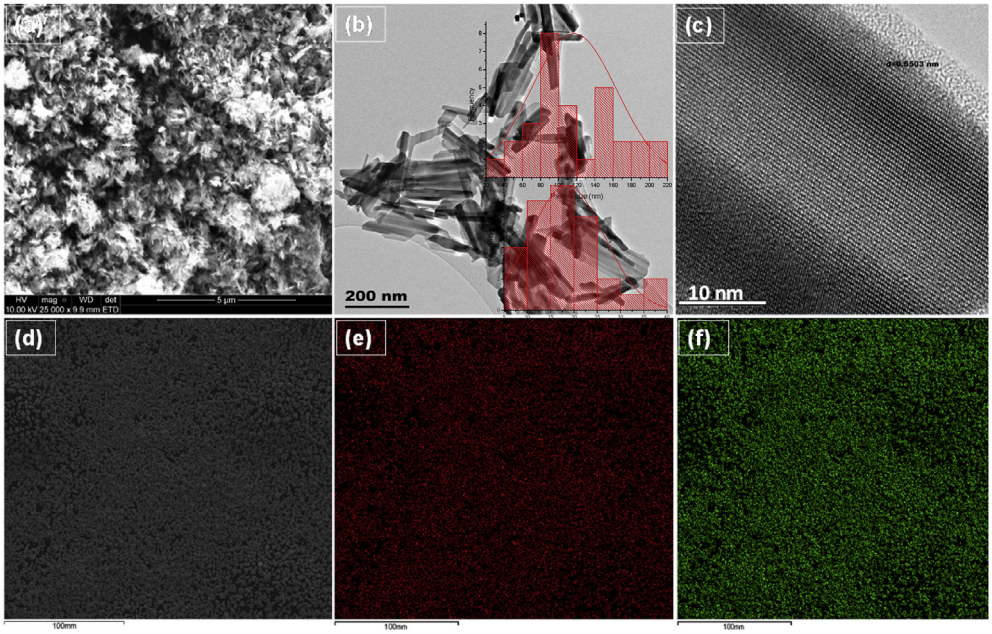

Figure 3. (a) SEM, (b) TEM, (c) HRTEM, (d) elemental mapping of Bi_2S_3 (e) Bi, and (f) S elements of Bi_2S_3(OAm) obtained in oleylamine.

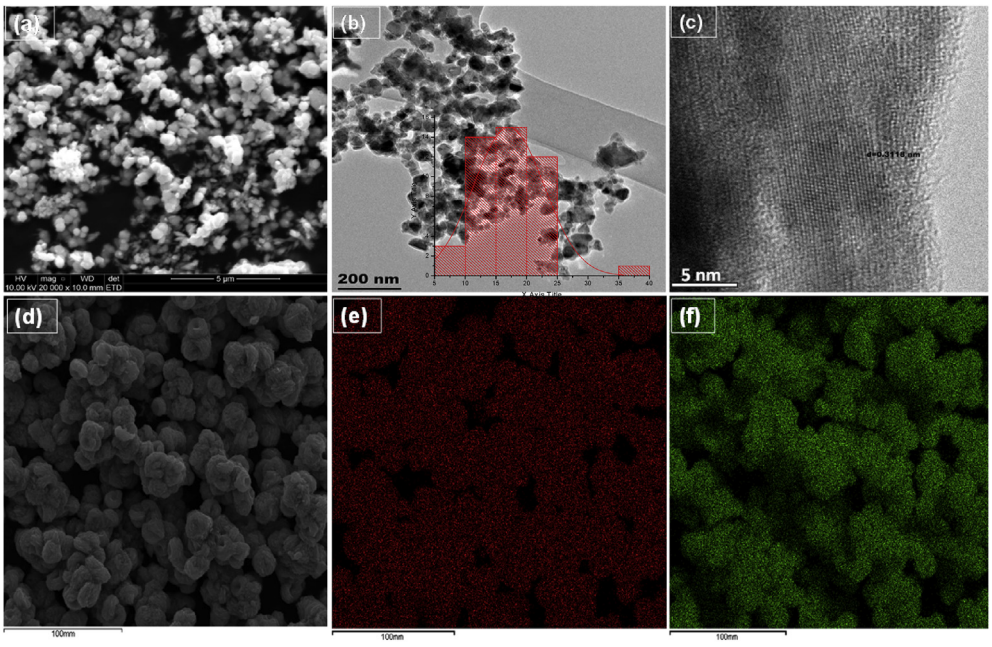

Figure 4. (a) SEM, (b) TEM, (c) HRTEM, (d) elemental mapping of Bi_2S_3 (e) Bi, and (f) S elements of Bi_2S_3(OAc) obtained in oleic acid.

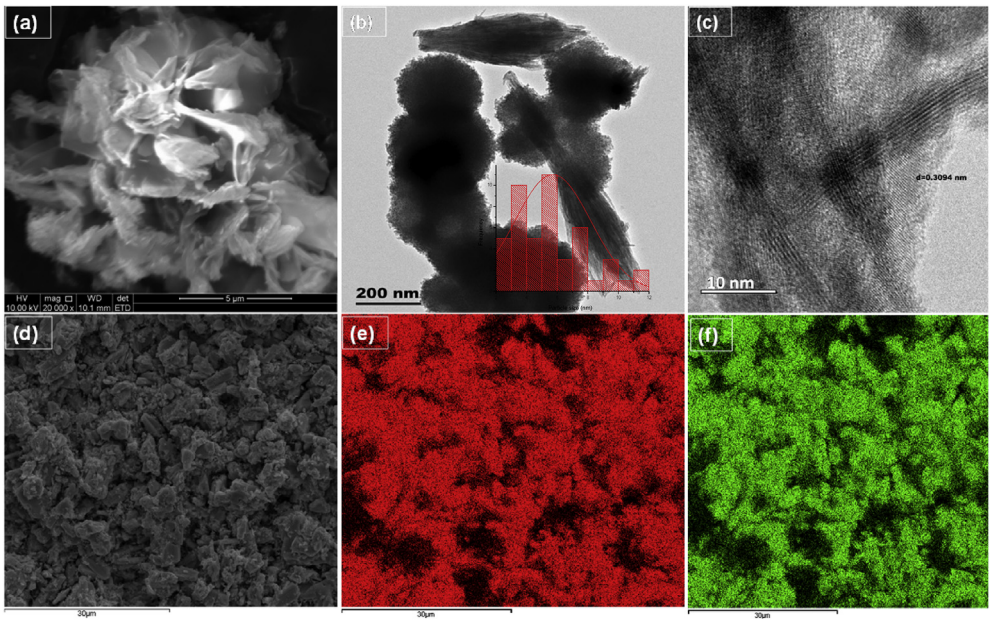

Figure 5. (a) SEM, (b) TEM, (c) HRTEM, (d) elemental mapping of Bi_2S_3 (e) Bi, and (f) S elements of Bi_2S_3(HDA) obtained in hexadecylamine.

spherical nanoparticles. The oleylamine and hexadecylamine have nitrogen as ligating atom, thus, the interaction of these ligands with bismuth cations in the solvothermal medium was relatively weaker compared to the oleic acid. This would allow for the growth of particles either via Ostwald ripening or oriented attachment. Thus, in Bi_2S_3(OAm) and Bi_2S_3(HDA), the possible preferential adsorption of ligands on certain facets of the nanoparticle surface might be one of the possible contributions to the anisiotropic morphology of the nanostructures.

The thermal decomposition of single source precursor in HDA has been reported to yield anisotropic morphologies of nanocrystals [54]. The mechanism of the nanostructure pattern has been attributed to the crystalline phase formation during nucleation, in addition to the growth rate difference between the surfaces of the crystal. These processes finally determine the overall structure of the nanostructure. Hexadecylamine could act both as a shape controlling ligand and also a stabilizing solvent. In the present study, HDA seems to enhance the growth rate towards one direction which resulted in ulthrathin Bi_2S_3 nanorods (Figure 5b).

The elemental mapping images in the (e) and (f) of Figures 3, 4, and 5 show that bismuth and sulphur were homogeneously distributed throughout the scan area of Bi_2S_3(OAm), Bi_2S_3(OAc), and Bi_2S_3(HDA), suggesting a good dispersion of the elemental composition of the nanostructures. The representative EDX spectrum presented in Figure 6 shows the distinct peaks corresponding to bismuth (Bi) and sulphur (S) and no impurity or extra peaks were detected which confirmed the high purity of the samples. The weight % of Bi and S present in Bi_2S_3(OAm), Bi_2S_3(OAc), and Bi_2S_3(HDA) are given as: 83.39, 16.61; 83.06, 16.94;

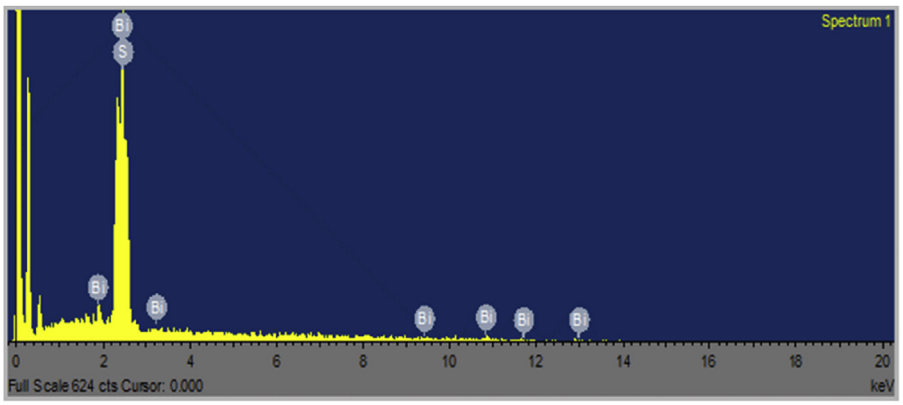

Figure 6. EDX spectrum of the as-prepared Bi_2S_3 using bismuth(III) tris(*N*-methyl-*N*-phenyldithiocarbamate) as single source precursor compound.

and 84.25, 15.75 respectively. The weight % of Bi and S in Bi_2S_3 is ideally expected to be 81.29 and 18.71% respectively. The obtained values are quite close to this, which revealed that the stoichiometric ratio of Bi to S was approximately 3:2. Although, the percentage Bi appeared slightly higher than the expected value and the slight percentage excess of Bi might be due to the absorption of excessive bismuth ions on the surface of nanomaterials [55]. Figure 7 demonstrates the fabrication of Bi_2S_3(OAm), Bi_2S_3(OAc), and Bi_2S_3(HDA) and their morphological variations. Significant differences in morphology are obvious for different capping materials used.

3.5. Optical studies

The UV–vis-NIR absorption and the corresponding photoluminescence spectra of the as-prepared Bi_2S_3(OAm), Bi_2S_3(OAc), and Bi_2S_3(HDA) samples are presented in Figure 8. As shown in Figure 8a, Bi_2S_3(OAm) has a maximum absorption around 565 nm, while the spectrum of Bi_2S_3(OAc) clearly show a broad band absorption, with peak around 300 nm (Figure 8b). The Bi_2S_3(HDA) exhibited a broad but low absorption which ranged from UV to visible region [32]. The energy band gap calculated from the Tauc plot of the respective $(\alpha h\nu)^2$

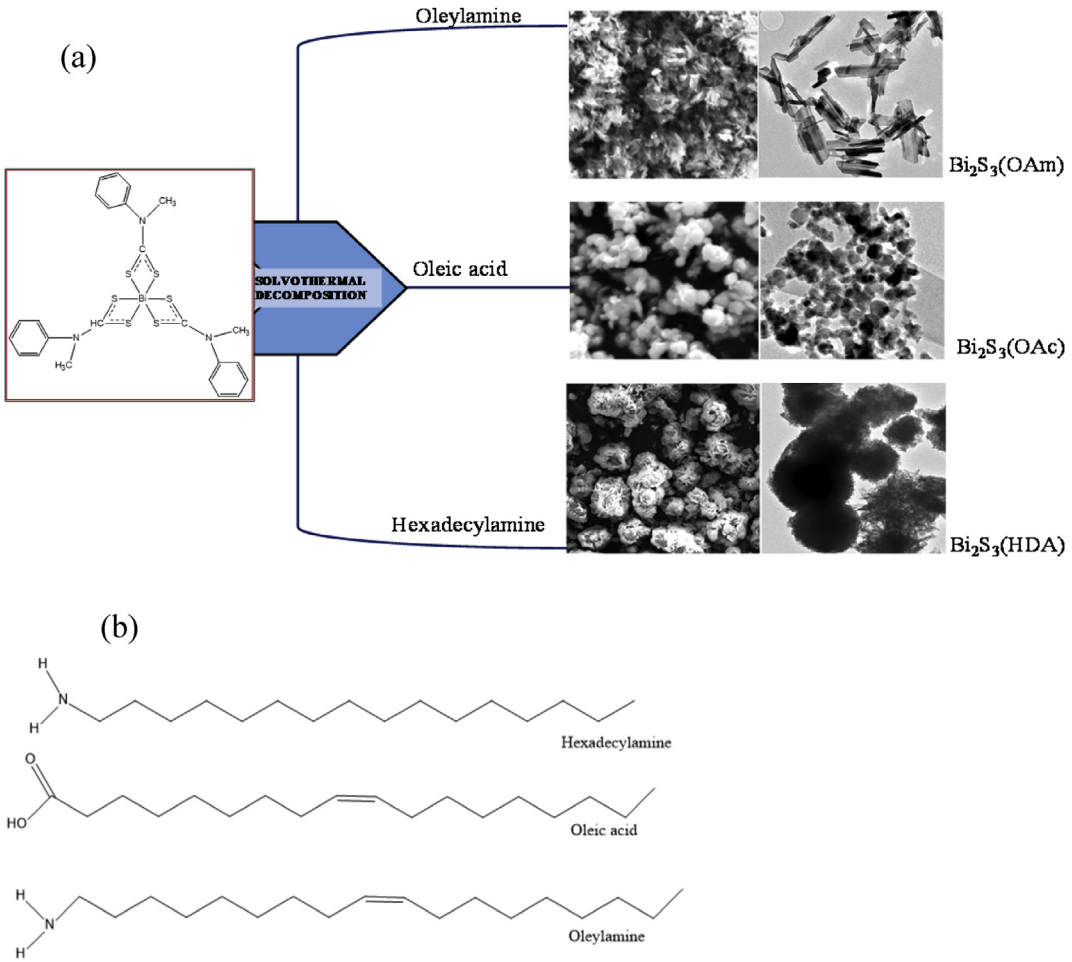

Figure 7. (a) Fabrication of Bi_2S_3(OAm), Bi_2S_3(OAc), and Bi_2S_3(HDA) and their shape variations with change in capping materials, (b) structures of the different capping ligands.

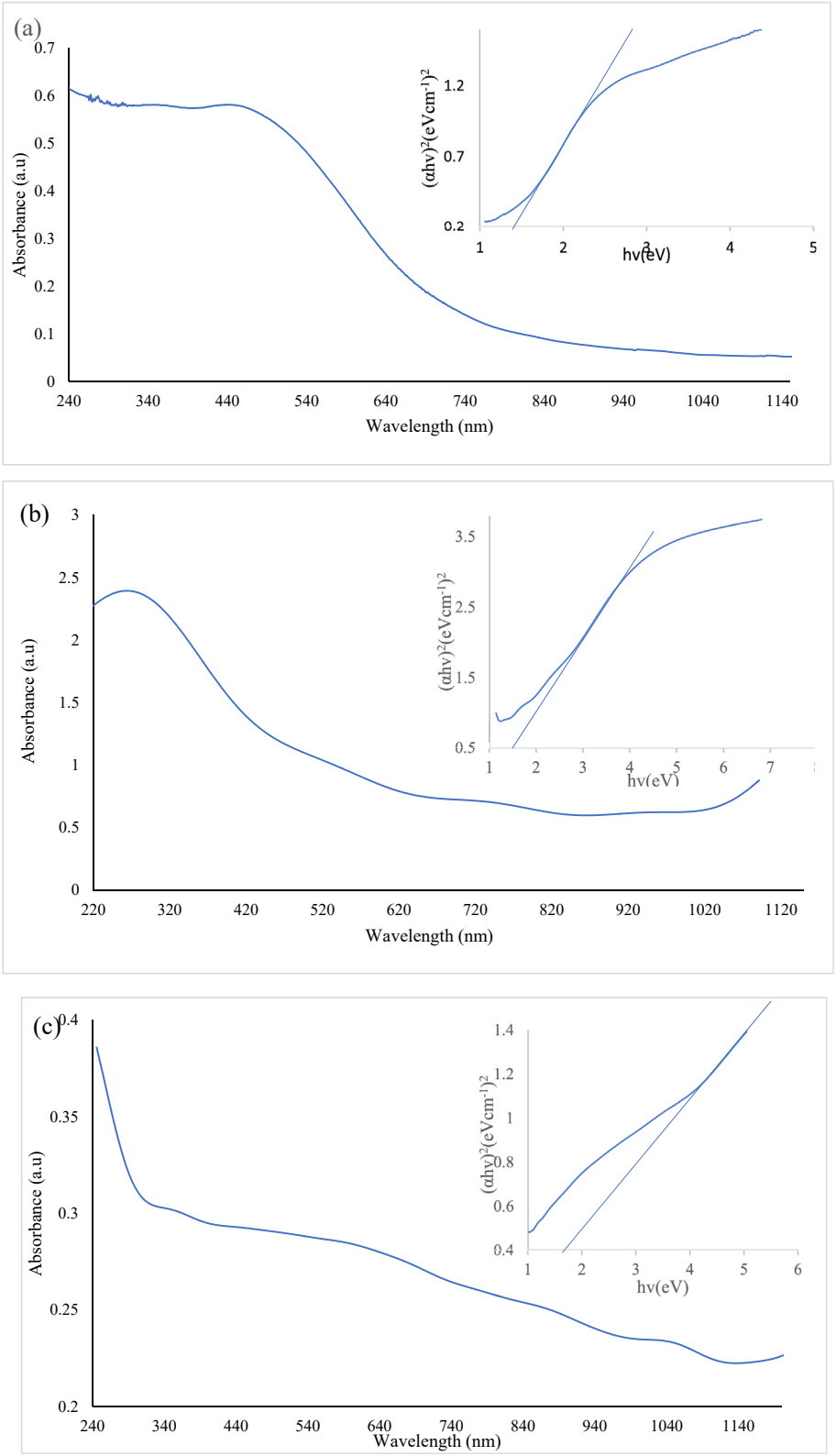

Figure 8. UV-vis-NIR and their respective Tauc plot of Bi_2S_3 synthesized using bismuth(III) tris(*N*-methyl-*N*-phenyldithiocarbamate) in (a) oleylamine-Bi_2S_3(OAm), (b) oleic acid-Bi_2S_3(OAc), and (c) hexadecylamine-Bi_2S_3(HDA).

vs. $h\nu$ (where α is the absorbance, h is Planck constant and ν is the frequency) gave the values 1.46, 1.50 and 1.72 eV for the Bi_2S_3(OAm), Bi_2S_3(OAc) and Bi_2S_3(HDA) respectively. These showed an increase in the energy band gap value of 1.3 eV reported of for bulk bismuth sulphide [56].

The photoluminescence (PL) spectra of the Bi_2S_3 at an excitation wavelength of 350 nm are presented in Figure 9, and they showed slight variation in intensity, broadness and positions of maximum peak. The photoluminescence spectra of the Bi_2S_3(OAm) exhibited a narrow peak at 615 nm with a weak broad shoulder at 665 nm, whereas Bi_2S_3(OAc) and

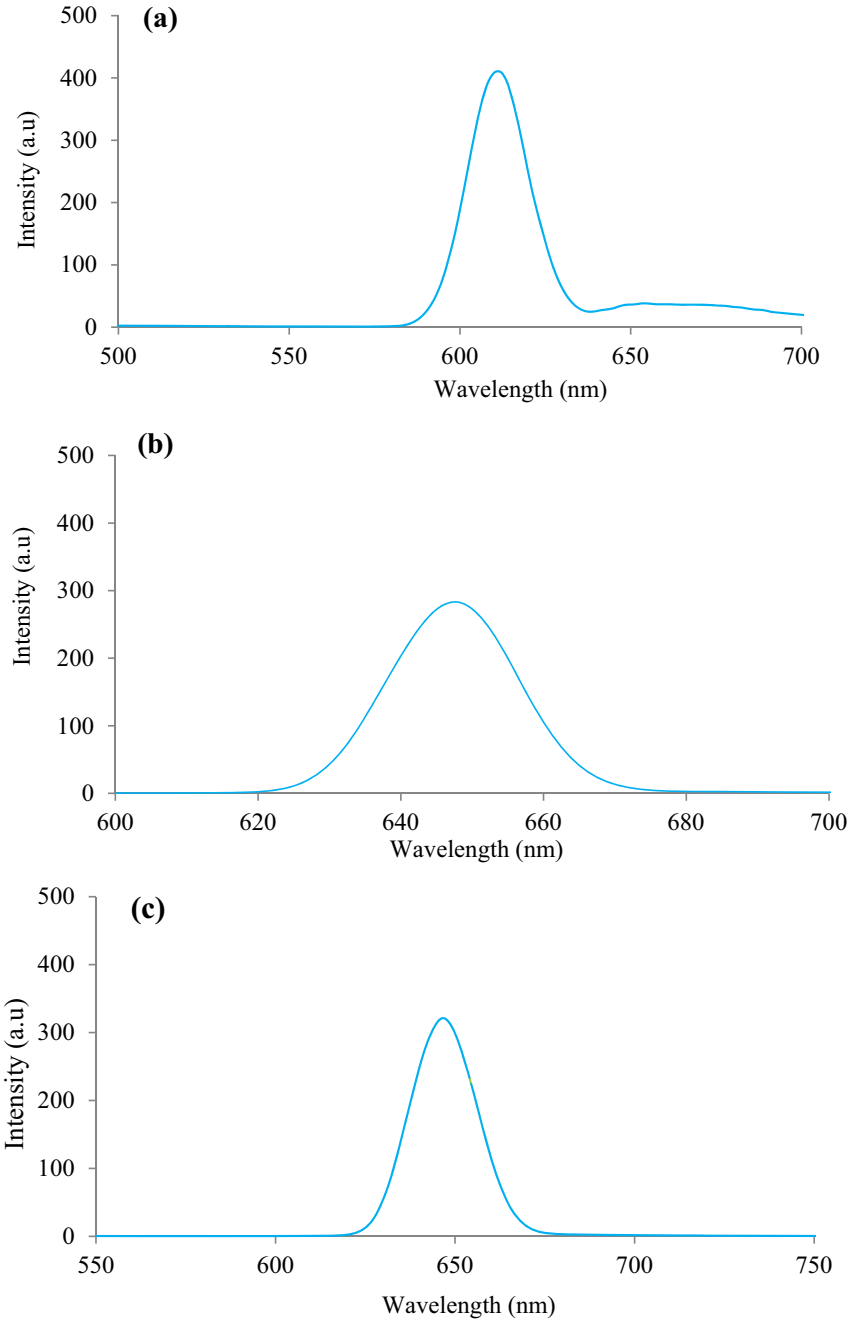

Figure 9. Photoluminescence spectra of Bi_2S_3 synthesized using bismuth(III) tris(*N*-methyl-*N*-phenyldithiocarbamate) in (a) oleylamine-Bi_2S_3(OAm), (b) oleic acid-Bi_2S_3(OAc), and (c) hexadecylamine-Bi_2S_3(HDA).

Bi_2S_3(HDA) nanostructures displayed only a peak at 646 and 648 nm respectively corresponding to band edge emission. In the spectra of Bi_2S_3(OAm) and Bi_2S_3(HDA) nanostructures, the narrow peak widths were indicative of narrow size distribution of the Bi_2S_3. In contrast, Bi_2S_3(OAc) showed a broad emission in the range 620–675 nm, with maximum at 646 nm. The accompanying broad shoulder in the spectrum of Bi_2S_3(OAm) may be indicative that a small portion of rods with different size distributions could also be present in addition to the nanorods that exhibited emission at 615 nm and the broadness of the peak could be attributed to a large distribution of the nanostructure [57, 58].

The optical properties of nanoparticles could be affected by factors which are inherent of the materials' properties such as the morphology, size, and concentration of the nanoparticles in solvent. In addition to this, external factors including the type of capping agents and dielectric constant of the solvent also play significant roles. In a solution of the nanoparticles, a charge transfer from the attached ligand molecules to nanoparticles could affect the optical and also the magnetic properties of the nanoparticles, and could cause a spectral shift [59]. Therefore, nanoparticles whose capping ligands contain functional groups such as amine, carbonyl and hydroxyl that act as electron donor or electron acceptor groups could form internal charge transfer states. Hence, with excitation there are possibilities of increase in charge separation within the nanoparticles. Furthermore, when there is an increase in the dielectric constant of the surrounding medium or solvent, the emission wavelength could shift to red or blue or even remains unaffected. The possibility of this shift or its extend is dependent on surface defects and therefore on the nature of the capping agent [60,61]. Other factors that

could affect the spectral shifts are the polarity and viscosity of the solvent, as well as changes in decay rates of radiative and non-radiative transitions [59]. The presence of some or all of these factors could make emission behaviour a complex phenomenon.

4. Conclusion

A variation in the morphology and size of bismuth sulphide nanoparticles was successfully achieved by using different solvents including oleylamine, oleic acid and hexadecylamine at 180 °C. XRD pattern showed that the crystallinity of the Bi_2S_3 was influenced by the solvent media, and a bias of orientations existed in the (2 1 1) crystallographic plane of the samples obtained using oleylamine. The TEM measurements showed that a significant difference occurred in the growth pattern and overall shape of nanoparticles due to the variation of solvents at uniform temperature and time of reaction. Since, the optical and electronic properties, which dictates the areas of application of different nanomaterials, is influenced by their morphology and structural properties, it implies that the synthesis of bismuth sulphide in oleylamine, oleic acid and hexadecylamine could be used to direct their growth patterns and areas of applications.

Declarations

Author contribution statement

Damian C. Onwudiwe: Conceived and designed the experiments; Analyzed and interpreted the data; Wrote the paper.

Violet M. Nkwe: Performed the experiments; Analyzed and interpreted the data.

Funding statement

This work was supported by financial assistance from the North-West University, South Africa and the National Research Foundation, South Africa (Grants Ref: UID109333 and UID 116338).

Competing interest statement

The authors declare no conflict of interest.

Additional information

No additional information is available for this paper.

References

[1] H. Zhong, Z. Bai, B. Zou, Tuning the luminescence properties of colloidal I–III–VI semiconductor nanocrystals for optoelectronics and biotechnology applications, J. Phys. Chem. Lett. 3 (2012) 3167–3175.

[2] D.V. Talapin, J.S. Lee, M.V. Kovalenko, E.V. Shevchenko, Prospects of colloidal nanocrystals for electronic and optoelectronic applications, Chem. Rev. 110 (2010) 389–458.

[3] X. Xin, M. He, W. Han, J. Jung, Low-cost copper zinc tin sulfide counter electrodes for high-efficiency dye-sensitized solar cells, Angew. Chem. Int. Ed. 50 (2011) 11739–11742.

[4] M.D. Regulacio, M.Y. Han, Composition-tunable alloyed semiconductor nanocrystals, Acc. Chem. Res. 43 (2010) 621–630.

[5] P. Devendran, T. Alagesan, A. Manikandan, S.A. Bahadur, M.K. Kumar, S. Rathinavel, K. Pandian, Sonochemical synthesis of Bi_2S_3 nanowires using single source precursor and their electrochemical activity, Nanosci. Nanotechnol. Lett. 8c (2016) 478–483.

[6] D.K. Manimegalai, A. Manikandan, S. Moortheswaran, S.A. Antony, One-pot microwave irradiation synthesis and characterization studies of nanocrystalline CdS photocatalysts, Adv. Sci. Eng. Med. 7 (2015) 722–727.

[7] A. Manikandan, S. Arul Antony, A novel approach for the synthesis and characterization studies of Mn^{2+} doped CdS nano-crystals by a facile microwave combustion method, J. Supercond. Nov. Magnetism 27 (2014) 2725–2733.

[8] K. Mokurala, A. Kamble, C. Bathina, P. Bhargava, S. Mallick, Effect of solvent, reaction time on morphology of Cu_2ZnSnS_4 (CZTS) nanoparticles and its application in Dye Sensitized Solar Cells, Mater. Today: Proceedings 3 (2016) 1778–1784.

[9] C. Neela Mohan, V. Renuga, A. Manikandan, Influence of silver precursor concentration on structural, optical and morphological properties of Cu1-xAgxInS2 semiconductor nanocrystals, J. Alloys Compd. 729 (2017) 407–417.

[10] V. Renuga, C. Neela Mohan, A. Manikandan, Influence of Mn^{2+} ions on both core/shell of $CuInS_2$/ZnS nanocrystals, Mater. Res. Bull. 98 (2018) 265–274.

[11] U. Ghorpade, M. Suryawanshi, S.W. Shin, K. Gurav, Patil, S. Pawar, S. Kolekar, Towards environmentally benign approaches for the synthesis of CZTSSe nanocrystals by a hot injection method: a status review, Chem. Comm. 50 (2014) 11258–11273.

[12] M.J. Thompson, T.P.A. Ruberu, K.J. Blakeney, K.V. Torres, P.S. Dilsaver, J. Vela, Axial composition gradients and phase segregation regulate the aspect ratio of Cu_2ZnSnS_4 nanorods, J. Phys. Chem. Lett. 4 (2014) 3918–3923.

[13] B. Lim, M.J. Tao, P.H.C. Camargo, Y. Zhu, Y. Xia, Shape- controlled synthesis of Pd nanocrystals in aqueous solutions, Adv. Funct. Mater. 19 (2009) 189–200.

[14] S.R. Chowdhury, P.S. Roy, S.K. Bhattacharya, Room temperature synthesis of polyvinyl alcohol stabilized palladium nanoparticles: solvent effect on shape and electro-catalytic activity, Nano-Struct. Nano-Objects 14 (2018) 11–18.

[15] Q. Ren, W. Wang, H. Shi, Y. Liang, Synthesis and shape-dependent visible-light-driven photocatalytic activities of Cu_2ZnSnS_4 nanostructures, Micro & Nano Lett. 9 (2014) 505–508.

[16] M. Miyauchi, T. Hanayama, D. Atarashi, E. Sakai, Photoenergy conversion in p-type Cu_2ZnSnS_4 nanorods and n-type metal oxide composites, J. Phys. Chem. C 116 (2012) 23945-–23950.

[17] S.S. Mali, P.S. Patil, C.K. Hong, Low-cost electrospun highly crystalline kesterite Cu_2ZnSnS_4 nanofiber counter electrodes for efficient dye-sensitized solar cells, ACS Appl. Mater. Interfaces 6 (2014) 1688–1696.

[18] W.C. Liu, B.L. Guo, X.S. Wu, F.M. Zhang, C.L. Mak, K.H. Wong, Facile hydrothermal synthesis of hydrotropic Cu_2ZnSnS_4 nanocrystalquantum dots: band-gap engineering and phonon confinement effect, J. Mater. Chem. 1 (2013) 3182–3186.

[19] T.S. Shyju, S. Anandhi, R.S. karthick, R. Gopalakrishnan, P. Kuppusami, Mechanosynthesis, deposition and characterization of CZTS and CZTSe materials for solar cell applications, J. Solid State Chem. 227 (2015) 165–177.

[20] V. Kumar, K. Singh, A. Kumar, M. Kumar, K. Singh, A. Vij, A. Thakur, Effect of solvent on crystallographic, morphological and optical properties of SnO_2 nanoparticles, Mater. Res. Bull. 85 (2017) 202–208.

[21] J. Ungula, B.F. Dejene, Effect of solvent medium on the structural, morphological and optical properties of ZnO nanoparticles synthesized by the sol–gel method, Physica B 480 (2016) 26–30.

[22] L.M. Peter, K.G.U. Wijayantha, D.J. Riley, J.P. Waggett, Band-edge tuning in self-assembled layers of Bi_2S_3 nanoparticles used to photosensitize nanocrystalline TiO_2, J. Phys. Chem. B 107 (2003) 8378–8381.

[23] N.-G. García-Peña, D. Díaz, G. Rodríguez-Gattorno, I. Betancourt, I. Zumeta-Dubé, Facile synthesis of rod-shaped bismuth sulfide@graphene oxide (Bi_2S_3@GO) composite, Mater. Chem. Phys. 219 (2018) 376–389.

[24] S. Zhou, J. Li, Y. Ke, S. Lu, Synthesis of bismuth sulfide nanorods in acidic media at room temperature, Mater. Lett. 57 (2003) 2602–2605.

[25] K. Biswas, L.-D. Zhao, G.M. Kanatzidis, Tellurium-free thermoelectric: the anisotropic n-type semiconductor Bi_2S_3, Adv. Energy Mater. 2 (2012) 634–638.

[26] R. Jin, G. Li, Y. Xu, J. Liu, G. Chen, Uniform Bi_2S_3 nanorods-assembled hollow spheres with excellent electrochemical hydrogen storage abilities, Int. J. Hydrogen Energy 39 (2014) 356–365.

[27] B. Xue, T. Sun, F. Mao, J. Xie, Gelatin-assisted green synthesis of bismuth sulfide nanorods under microwave irradiation, Mater. Lett. 122 (2014) 106–109.

[28] S. Yu, Y. Qian, L. Shu, Y. Xie, L. Yang, C. Wang, Solvent thermal synthesis and characterization of ultrafine powder of bismuth sulfide, Mater. Lett. 35 (1998) 116–119.

[29] A. Sarkar, A.B. Ghosh, N. Saha, D.N. Srivastava, P. Paul, B. Adhikary, Enhanced photocatalytic performance of morphologically tuned Bi_2S_3 NPs in the degradation of organic pollutants under visible light irradiation, J. Colloid Interf. Sci. 483 (2016) 49–59.

[30] F. Chen, Y. Cao, D. Jia, Facile synthesis of Bi_2S_3 hierarchical nanostructure with enhanced photocatalytic activity, J. Colloid Interf. Sci. 404 (2013) 110–116.

[31] M. Salavati-Niasari, D. Ghanbari, F. Davar, Synthesis of different morphologies of bismuth sulfide nanostructures via hydrothermal process in the presence of thioglycolic acid, J. Alloys Compd. 488 (2009) 442–447.

[32] J. Chao, S. Xing, Y. Zhao, S. Gao, Q. Song, L. Guo, D. Wang, T. Zhang, Bismuth sulfide nanoflakes and nanorods as high performance photodetectors and photoelectrochemical cells, Solid State Sci. 61 (2016) 51–57.

[33] A.M. Palve, Deposition of zinc sulfide thin films from zinc(II) thiosemicarbazones as single molecular precursors using aerosol assisted chemical vapor deposition technique, Front. Mater. 6 (2019) 1–7.

[34] P. Devendran, T. Alagesan, T.R. Ravindran, K. Pandian, Synthesis of spherical CdS quantum dots using cadmium diethyldithiocarbamate as single source precursor in olive oil medium, Curr. Nanosci. 10 (2014) 302–307.

[35] G. Hogarth, Transition metal dithiocarbamates: 1978–2003, in: K.D. Karlin (Ed.), Progress in Inorganic Chemistry, 53, Wiley, Hoboken, NJ, 2005, pp. 71–561.

[36] N. Hollingsworth, A. Roffey, H.-U. Islam, M. Mercy, A. Roldan, W. Bras, M. Wolthers, C.R.A. Catlow, G. Sankar, G. Hogarth, N.H. de Leeuw, The active nature of primary amines during the thermal decomposition of nickel-dithiocarbamates to nickel-sulfide nanoparticles, Chem. Mater. 26 (2014) 6281–6292.

[37] N.O. Boadi, M.A. Malik, P. O'Brien, J.A.M. Awudza, Single source molecular precursor routes to lead chalcogenides, Dalton Trans. 41 (2012) 10497–10506.

[38] T. Trindade, P. O'Brien, Synthesis of CdS and CdSe nanoparticles by thermolysis of diethyldithio-or diethyldiseleno-carbamates of cadmium, J. Mater. Chem. 6 (1996) 343–347.

[39] M.A. Malik, N. Revaprasadu, P. O'Brien, Air-stable single-source precursors for the synthesis of chalcogenide semiconductor nanoparticles, Chem. Mater. 13 (2001) 913–920.
[40] J.R. Brent, P.D. McNaughter, P. O'Brien, Precursor determined lateral size control of monolayer MoS_2 nanosheets from a series of alkylammonium thiomolybdates: a reversal of trend between growth media, Chem. Comm. 53 (2017) 6428–6431.
[41] M.P. Motaung, J. Osuntokun, D.C. Onwudiwe, The heat-up synthesis of monodispersed Bi_2S_3 and Cu_7S_4 nanoparticles from novel precursor complexes and their characterizations, Mater. Sci. Semicond. Process. 99 (2019) 92–98.
[42] C. Gervas, S. Mlowe, M.P. Akerman, I. Ezekiel, T. Moyo, N. Revaprasadu, Synthesis of rare pure phase Ni3S4and Ni3S2nanoparticles in differentprimary amine coordinating solvents, Polyhedron 122 (2017) 16–24.
[43] E.M. Nagy, S. Sitran, M. Montopoli, M. Favaro, L. Marchio, L. Caparrotta, D. Fregona, Zinc(II) complexes with dithiocarbamato derivatives: structural characterisation andbiological assays on cancerous cell lines, J. Inorg. Biochem. 117 (2012) 131–139.
[44] X.G. Peng, Mechanisms for the shape-control and shape-evolution of colloidal semiconductor nanocrystals, Adv. Mater. 15 (2003) 459–463.
[45] Y. Sun, Y. Xia, Mechanistic study on the replacement reaction between silver nanostructures and chloroauric acid in aqueous medium, J. Am. Chem. Soc. 126 (2004) 3892–3901.
[46] W.H. Li, Synthesis and characterization of bismuth sulfide nanowires through microwave solvothermal technique, Mater. Lett. 62 (2008) 243–245.
[47] Z. Liu, J. Liang, S. Li, S. Peng, Y. Qian, Synthesis and growth mechanism of Bi_2S_3 nanoribbons, Chem. Eur J. 10 (2004) 634–640.
[48] J. Zhong, W. Xiang, L. Liu, X. Yang, W. Cai, J. Zhang, X. Liang, Biomolecule-assisted solvothermal synthesis of bismuth sulfide nanorods, J. Mater. Sci. Technol. 26 (2010) 417–422.
[49] S. Mourdikoudis, L.M. Liz-Marzan, Oleylamine in nanoparticle synthesis, Chem. Mater. 25 (2013) 1465–1476.
[50] K. Liu, Z.R. Shen, Y. Li, S.D. Han, T.L. Hu, D.S. Zhang, X.H. Bu, W.J. Ruan, Solvent induced rapid modulation of micro/nano structures of metal carboxylates coordination polymers: mechanism and morphology dependent magnetism, Sci. Rep. 4 (2014) 6023.
[51] O. Khani, H.R. Rajabi, M.H. Yousefi, A.A. Khosravi, M. Jannesari, M. Shamsipur, Synthesis and characterizations of ultra-small ZnS and Zn(1x)FexS quantum dots in aqueous media and spectroscopic study of their interactions with bovine serum albumin, Spectrochim. Acta, Part A 79 (2011) 361–369.
[52] T. Hemalatha, S. Akilandeswari, Synthesis and characterization of hmta assisted cuo nanoparticles with its potential antibacterial application, Int. J. Recent Sci. Res. 6 (2015) 7502–7507.
[53] H.M. Zheng, R.K. Smith, Y.W. Jun, C. Kisielowski, U. Dahmen, A.P. Alivisatos, Observation of single colloidal platinum nanocrystal growth trajectories, Science 324 (2009) 1309–1312.
[54] Y.W. Jun, S.M. Lee, N.J. Kang, J. Cheon, Controlled synthesis of multi-armed CdS nanorod architectures using monosurfactant system, J. Am. Chem. Soc. 123 (2001) 5150–5151.
[55] S. Yadav, K. Shrivas, P.K. Bajpai, Role of precursors in controlling the size, shape and morphology in the synthesis of copper sulfide nanoparticles and their application for fluorescence detection, J. Alloys Compd. 772 (2019) 579–592.
[56] E.B. Díaz-Cruz, O.A. Castelo-González, C. Martínez-Alonso, Z. Montiel-González, M.C. Arenas-Arrocena, Hailin Hu, Morphology control in microwave synthesized bismuth sulfide by using different bismuth salts, Mater. Sci. Semicond. Process. 75 (2018) 311–318.
[57] V.I. Klimov, Optical nonlinearities and ultrafast carrier dynamics in semiconductor nanocrystals, J. Phys. Chem. B 104 (2000) 6112–6123.
[58] J.B. Biswal, S.S. Garje, J. Nuwad, C.G.S. Pillai, Bismuth(III) dialkyldithiophosphates: facile single source precursors for the preparation of bismuth sulfide nanorods and bismuth phosphate thin films, J. Solid State Chem. 204 (2013) 348–355.
[59] D.Y. Inamdar, S.R. Vaidya, S. Mahamuni, On the photoluminescence emission of ZnO, Nanocrystals, J. Exp. Nanosci. 9 (2014) 533–540.
[60] J.R. Lakowicz, Principles of Fluorescence Spectroscopy, Springer, New York, 2006.
[61] M.L. Singla, M.M. Shafeeq, M. Kumar, Optical characterization of ZnO nanoparticles capped with various surfactants, J. Lumin. 129 (2008) 434–438.